Conformational Preferences in the Transition States and Tetrahedral Intermediates of Transacylations. Relationships to Enzyme-Bound Conformations of Phosphonate Inhibitors of Lipases and Esterases

Yu Takano and K. N. Houk*

Department of Chemistry and Biochemistry, University of California, Los Angeles, California 90095-1569

Received: September 11, 2004

The mechanism of the transacylation reaction of methyl acetate with methoxide has been explored using density functional theory (B3LYP/6-31+G(d)) and PCM−UAKS solvation models. The conformations of all of the transition states and intermediates are strongly influenced by the anomeric effect. The conformations of phosphonates were computed and analyzed. The bound inhibitors obtained from X-ray crystallographic structures of lipases and esterases adopt a few specific conformations. The conformers of the transition states and intermediates in transacylations are compared to the conformations of the phosphonate inhibitors. Although the energy differences are small, the frequency of the occurrence of the phosphonate conformers in crystal structures is more closely related to the relative energies of free phosphonate conformers than to the relative energies of acylation transition states.

Introduction

A central tenet in the field of enzyme inhibition is that effective inhibitors resemble the transition state of the reaction catalyzed by the enzyme.[1a] This form of molecular recognition is one type of complementarity between small molecules and proteins that is very important in chemical biology.[1] Because of the relatively restricted nature of the interior of an active site of an enzyme, limited conformational freedom is expected for a bound inhibitor or transition state.[2] The research described in this paper was designed to answer the following questions:

(1) Does the transition state of an enzyme-catalyzed reaction resemble the lowest energy transition state of a conformationally flexible system in solution?

(2) Do conformationally flexible enzyme inhibitors have conformations resembling the lowest energy conformation of transition state of the inhibited reaction?

Three-dimensional X-ray crystallographic structures of lipases and esterases from several different species show striking similarities to each other. In particular, the bound phosphonate inhibitors exist in only a few of the possible conformations.[3,4] The relationships between the conformations of the transition states and tetrahedral intermediates for the transacylations and the conformations of the unbound and bound inhibitors have been explored to understand how these conformational factors are related to catalysis by enzymes.

The parent transacylation reaction, $MeO^- + MeCO_2Me \rightarrow MeCO_2Me + MeO^-$, has been explored theoretically to understand the conformations of the transition states and intermediates in transacylations. The conformations of the transition states and intermediates have been compared to those of unbound phosphonates, as well as phosphonate inhibitors bound to lipases and esterases. The goal of this work is to determine which conformations are favored in the transacylation process and to explore the relationship, if any, to the observed conformations of the bound inhibitors. We find that energy differences among conformers are small in both transacylations and phosphonates. To the extent that there is a correlation, bound phosphonate conformations in enzyme crystals more closely resemble free phosphonate conformers than they do transacylation transition-state conformers.

* Author to whom correspondence should be addressed. E-mail: houk@chem.ucla.edu.

Background

Lipases and Esterases. Lipases and esterases have been found in most organisms. These enzymes catalyze the transacylation and deacylation reactions of esters involved in bioconversion reactions.[3] In addition to their biological functions, they are probably the most useful enzymes in synthetic organic chemistry, catalyzing the chemoselective, regioselective, and/or stereoselective hydrolysis of esters. The broad synthetic potential of these enzymes is largely due to the fact that lipases and esterases accept a wide range of substrates, and they are quite stable in either aqueous or nonaqueous organic solvents.[3]

Crystal Structures of Lipases and Esterases. The X-ray crystal structures of several lipases and esterases have been reported.[4] Most lipases and esterases are members of the "α/β-hydrolase fold family". Lipases and esterases differ widely in size, ranging from 22 kD for *Fusarium solani* cutinase to 60 kD for *Geotrichum candidum* lipase.[4] The three-dimensional structures of lipases and esterases are very similar, despite major differences in the amino acid sequences.[4] This α/β-hydrolase folding pattern arranges the residues of a catalytic triad (typically, Ser, His, and either Glu or Asp) in an identical manner, as shown in Figure 1. This figure also shows the crystal structures of inhibitors bound in the active site. The nucleophilic Ser rests at a hairpin turn between a β-strand and an α-helix. The remaining residues of the catalytic triad rest on one side of the serine. The residues forming the oxyanion hole, which has also been identified on the basis of the X-ray structures, lie on the other side. A notable exception is *Streptomyces scabies* esterase.[4c] The tertiary fold of the enzyme is different from those of the α/β-hydrolase fold family. Furthermore, the active site

10.1021/jp045889a CCC: $27.50
Published on Web 12/08/2004

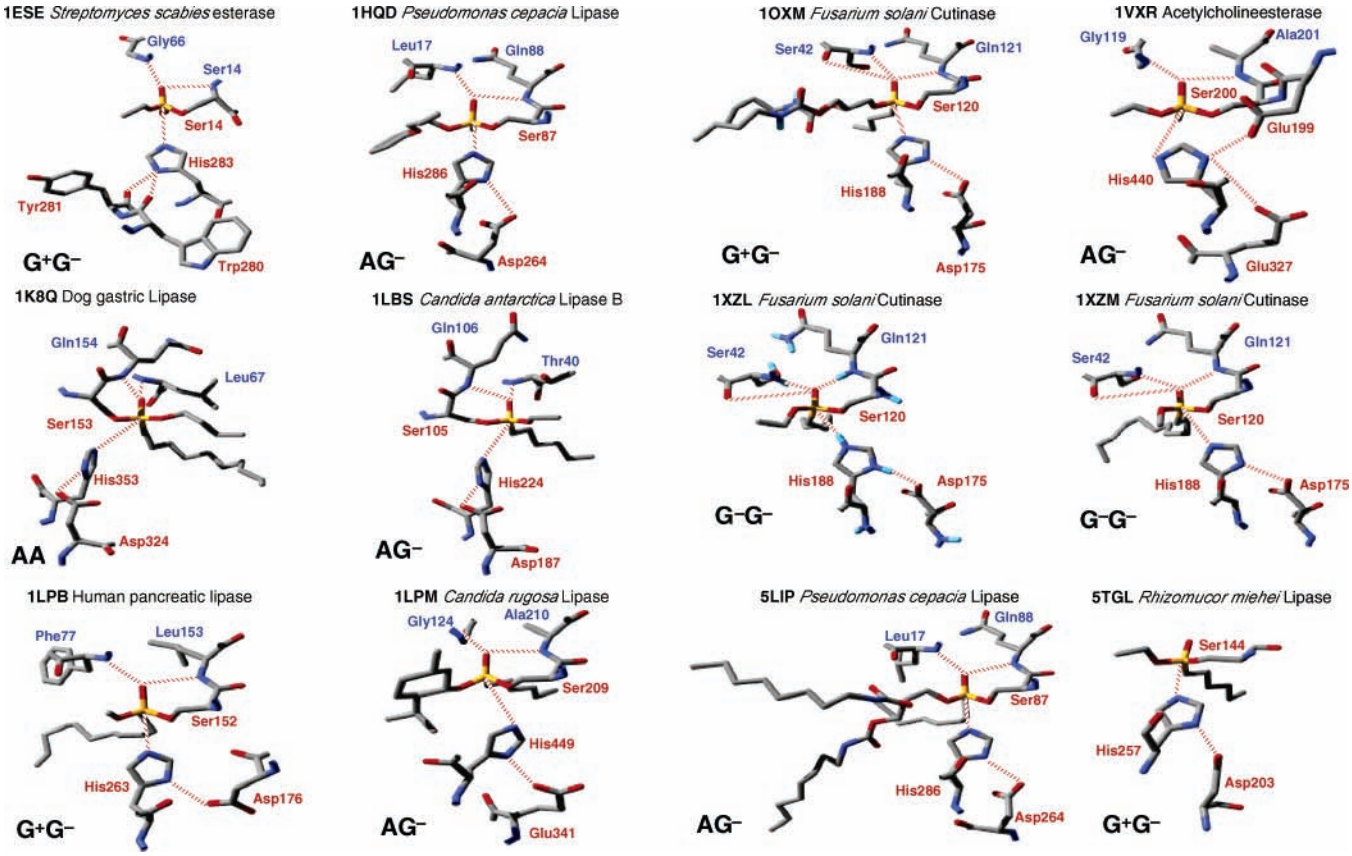

Figure 1. X-ray crystallographic structures of the active site of lipases and esterases inhibited by phosphonates. Residues that constitute an oxyanion hole and a catalytic triad are shown in blue and red, respectively. $\mathbf{G^+G^-}$, $\mathbf{AG^-}$, $\mathbf{G^-G^-}$, and **AA** refer to the phosphonate conformations discussed in the text. Three $\mathbf{G^+G^-}$ inhibitors are not shown, because these structures have not been published yet (see ref 4n).

contains a dyad of Ser14 and His283, but a Glu or Asp part is replaced by a natural hydrogen-bond acceptors (Trp280 and Tyr281).[4c] The conformations of the bound phosphonates are of special interest and are discussed in detail later in this paper.

Mechanism of the Hydrolysis of Esters by Lipases and Esterases. The X-ray structures of lipases and esterases with the bound inhibitors yield valuable information about the mechanism of the transacylation and deacylation reactions catalyzed by this enzyme family.[4] The essential catalytic functional unit in the active site is the catalytic triad.[3−6] The residues Ser and His serve as a nucleophilic attacking group and a general acid−base catalyst, respectively. The catalytic role of the third residue of the catalytic triad is still controversial.[6] Recent quantum mechanics/molecular mechanics (QM/MM) calculations have suggested that the electrostatic interaction between the third residue and His stabilizes the transition state and tetrahedral intermediate.[6f,g] A prototypical catalytic mechanism is shown in Scheme 1. The first chemical step is the attack of Ser at the ester carbonyl, forming a tetrahedral intermediate. The oxyanion hole stabilizes the negative charged transition state and tetrahedral intermediate during catalysis. The intermediate then collapses to give the acyl enzyme, releasing the alcohol in a transacylation.[3,4] The acyl enzyme undergoes the hydrolysis to form the carboxylic acid and to regenerate the serine on the enzyme.

Theoretical Studies of the Acyl Substitution Reactions. There have been many computational studies of nucleophilic acyl substitutions.[5c,7] Jorgensen studied the reaction of the hydroxide ion with methyl formate.[7a] Dewar and Storch reported AM1 calculations for the reactions of seven anions with eight carboxylic derivatives, suggesting that the activation barriers in solution correspond to the energy needed to desolvate the

SCHEME 1

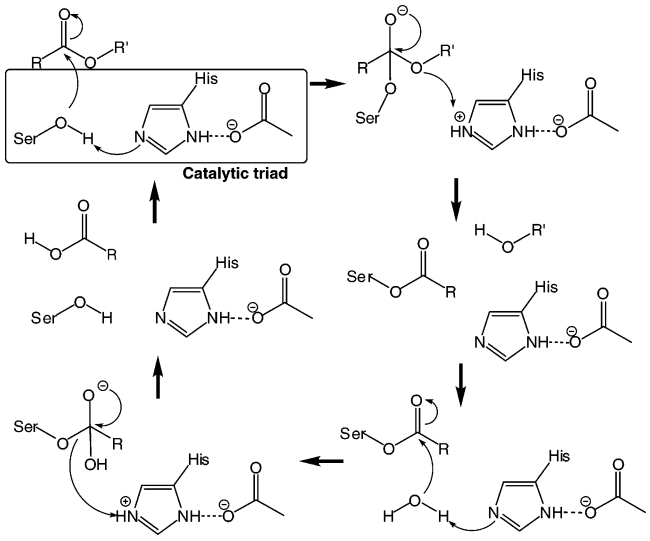

nucleophilic anion,[7b] and Hori studied the decomposition of the tetrahedral intermediate at the MP2/6-31+G(d,p)//HF/6-31+G level of theory.[7c] Pranata studied the gas-phase base-catalyzed hydrolysis of methyl formate, finding two tetrahedral intermediates along the reaction pathway,[7d] and Hæffner et al. investigated the mechanism of the base-catalyzed hydrolysis of methyl acetate at the MP2/6-31+G(d)//HF/6-31+G(d) level.[7e] The stepwise mechanism was favored over the concerted one by 5.3 and 13.3 kcal/mol in the gas phase and water, respectively. Sherer, Turner, and Shields investigated the first step of the reaction with semiempirical and ab initio molecular orbital methods.[7f,g] Tantillo and Houk explored the alkaline hydrolysis

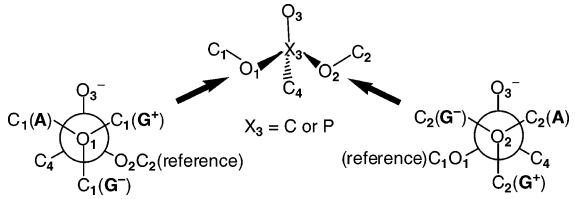

Figure 2. Molecular structure and conformational definition of the tetrahedral intermediates in transacylations and the conformers of dimethyl methylphosphonate.

of aryl esters in both the gas phase and water at the MP2/6-31+G(d)//HF/6-31+G(d) theory,[5c] showing that the mechanism was a concerted reaction in the gas phase but a stepwise addition−elimination reaction in water. Chong et al. explored the hydrolysis of *p*-nitrophenyl acetate and *p*-nitroacetoanilide through the B3LYP/6-31+G(d) calculation, molecular dynamics simulation, and MM-PBSA free energy calculations.[7h] Zhan, Landry, and Ornstein studied the reaction pathways for alkaline hydrolysis of carboxylic acid esters in the gas phase and water.[7i−k] Pliego and Riveros reported the free energy profile for the different reaction pathways available to the hydroxide and methyl formate in water and dimethylsulfoxide (DMSO).[7l−n] They suggested that the tetrahedral intermediate was formed by a direct nucleophilic attack of the hydroxide on the carbonyl carbon or by a general base catalysis mechanism.

Stereoelectronic Effects for the Cleavage of Tetrahedral Intermediates. Deslongchamps analyzed the stereoelectronic effects that control the cleavage of tetrahedral intermediates during the formation or hydrolysis of esters and amides.[8a] His book provides guidelines to the understanding of which conformations of tetrahedral intermediates are most prone to cleavage. Ema and co-workers performed semiempirical molecular orbital (MO) calculations on the imidazole-catalyzed transesterification and suggested that the stabilization energy that was due to the stereoelectronic effect operating at the transition state was ∼5 kcal/mol.[8b] However, Perrin investigated the hydrolysis of cyclic amidines and suggested that the antiperiplanar lone-pair hypothesis cannot always account for the preferred reaction pathways of tetrahedral intermediates.[8c]

Our study was designed (i) to elucidate why the phosphonate inhibitors bound in lipases and esterases prefer only a few conformations and (ii) to determine the relationship to conformations of species that are involved in transacylations.

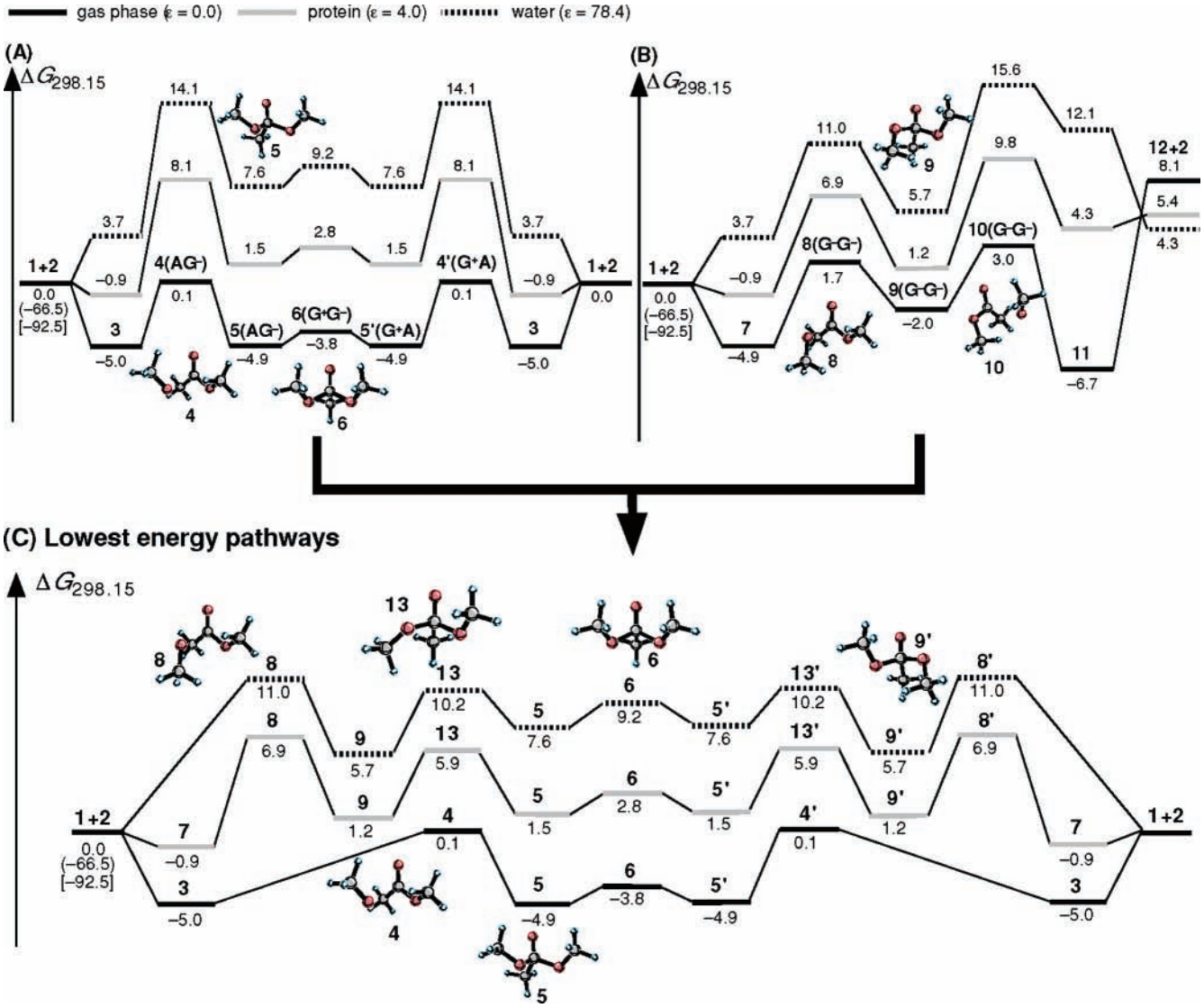

Figure 3. Reaction pathways for the transacylation of methyl acetate via (A) the **AG**$^-$ and (B) **G**$^-$**G**$^-$ tetrahedral intermediates and (C) the lowest energy pathways in the gas phase, protein, and water. Gibbs free energies of B3LYP/6-31+G(d) stationary points are plotted, relative to that of reactants (**1** + **2**). Solvation free energies in water and nonpolar protein environments with the PCM−UAKS method are given in parentheses and brackets, respectively. The relative Gibbs free energies are given in units of kcal/mol.

Computational Methods

The reaction pathways for the transacylation of methyl acetate with methoxide anion were explored at the B3LYP/6-31+G(d)[9−11] level, using Gaussian 98.[12a,13] All stationary points and transition states were characterized by frequency calculations at the B3LYP/6-31+G(d) level, and zero-point energies and thermal corrections at 298 K (scaled by 0.98)[14] were included.

Solvation energies were computed with PCM−UAKS self-consistent reaction field (SCRF) single-point calculations[15] at the HF/6-31+G(d) level, using Gaussian 03.[12b] In Gaussian 03, the PCM solvation method has been improved and extended.[15c] Dielectric constants (ϵ) of 78.39 and 4 were used,[16] to simulate the higher-polar aqueous environment and a less-polar environment due to that of a protein interior, respectively. We neglected the rotational and the translational contributions to the thermal energies and entropies for complexes, transition states, and intermediates when the thermal and entropy corrections to the free energies in solution were computed, because the ability of the solute to move around in the solvent can be assumed to be restricted.[7c]

The conformations of the transition states and tetrahedral intermediates for the transacylation are defined as the anti (**A**), gauche$^+$ (**G**$^+$), or gauche$^-$ (**G**$^-$) designations, to show the relationships of the alkoxy groups O_1C_1 and O_2C_2, with respect to the O_2X_3 and O_1X_3 bonds, respectively (Figure 2). These correspond to a staggered arrangement with dihedral angles of ∼180°, 60°, and −60°, respectively. One also could have defined the OC dihedral angle, with respect to X_3O_3, and the relationship will be discussed in the text.

The Mechanism of Transacylation of Methyl Acetate

Transacylation via the AG$^-$ Tetrahedral Intermediate. The reaction of methyl acetate with methoxide was explored at the B3LYP/6-31+G(d) level under vacuum and in water and protein environments.[17] Figure 3A shows the lowest-energy pathway for the gas-phase reaction. Gas-phase geometries of all of the stationary points are shown in Figure 4. Table 1 lists the entropy corrections that are involved in the transacylation. The approach of methoxide **2** to the *Z* isomer of methyl acetate **1** forms an ion−molecule complex (**3**). In **3**, the methoxide oxygen can be hydrogen-bonded to one of the H atoms of the methyl group (CH···O), with a distance of 1.63 Å. CH···O hydrogen bonds become increasingly important for the understanding of conformational analyses and intermolecular interactions. The CH···O bond is, similar to the OH···O hydrogen bonds, a largely electrostatic interaction.[18] The O_1C_1 distance elongates to 1.36 Å, because of the CH···O hydrogen bond. Attack of the methoxide on methyl acetate leads to a tetrahedral intermediate (**5**) via a rate-determining transition state (**4**). Transition state **4** has the **AG**$^-$ geometry, with the methoxide approaching anti to the ester O_2C_3 bond, whereas the ester methoxy (O_2C_2) rotates into a **G**$^-$ arrangement, with respect to the newly forming bond. Transition state **4** involves the methoxide lone-pair interaction with the carbonyl π^* orbital. The intermediate **5** has the same **AG**$^-$ conformation as the transition state. The formation of the O_1C_3 bond causes an increase of the O_2C_3 distance by 0.14 Å. The angle of attack ($O_1C_3O_3$) shifts from 102° in **4** to 114° in **5**. The dihedral angle $O_3C_3O_2C_2$ of the ester gradually changes from 0° in **1** to 42° (**G**$^-$) in **5**. The O_1C_3 bond length is different from the O_2C_3 bond length, because of the anomeric effect.[19] The **AG**$^-$ intermediate can isomerize to its mirror image (**5′**), **G**$^+$**A**, through transition state **6**. Transition state **6** has **G**$^+$**G**$^-$ conformation and is only 1.1 kcal/mol above **5**, because of the 1.2 kcal/mol difference in the entropy corrections ($-T\Delta S$; see Table 1). In the change of **5** to **6**, the O_1C_3 bond shrinks by 0.03 Å for the **A**-methoxy group and elongates by 0.04 Å for the **G**$^-$-methoxy group, whereas almost no change in the length of the carbonyl O_3C_3 bond is observed. The dihedral angle $O_3C_3O_2C_2$ shifts from 42° in **5** to 28° in **6** as the **G**$^-$-methoxy group (O_2Me) responds to the steric hindrance to the other **G**$^+$-methoxy group (O_1Me). Finally, the dissociation of the **A**-methoxy group of **5′** completes the transacylation. Overall, the process is essentially barrierless in the gas phase, and the two halves of the reaction are mirror images and, therefore, are of equal energy.

TABLE 1: Entropy Corrections to the Gibbs Free Energies of B3LYP/6-31+G(d) Stationary Points in the Transacylation of Methyl Acetate in the Gas Phase

component	Gibbs free energy correction, $-T\Delta S$ at 298.15 K (kcal/mol)
1 + **2**	−39.8
3	−30.4
4	−28.6
5	−27.2
6	−26.0
7	−30.3
8	−28.1
9	−26.9
10	−28.0
11	−30.9
12 + **2**	−39.3
13	−25.7

In the aqueous environment or the nonpolar environment representing the extreme of a hydrophobic protein interior, the energy of unassociated reactants (**1** + **2**) is stabilized by 92.5 and 66.5 kcal/mol, respectively. The calculated aqueous solvation free energy for methyl acetate is −4.7 kcal/mol, which is similar to the experimental value (−3.1 kcal/mol),[20] indicating that the PCM is reasonably close to the experiment for this case. In a nonpolar protein interior, **1** and **2** form the complex **3**, but the stabilization energy is only 0.9 kcal/mol. Solvation effects make complex **3** irrelevant in water. The formation of **5** from **1** and **2** is endothermic with a $\Delta G^{\ddagger}$ value of 14.1 and 8.1 kcal/mol for water or nonpolar solvents. The solvation effects slightly influence the activation barrier for interconversion of **5** and **5′** via **6**, and the intermediate has a shallow conformational barrier where both methoxy groups can freely sample the **AG**$^-$−**G**$^+$**G**$^-$−**G**$^+$**A** conformational space in the gas phase, protein, and water.

Transacylation via the G$^-$G$^-$ Tetrahedral Intermediate. There is a second transition state for nucleophilic attack, as shown in Figure 3B. An isomeric ion−molecule complex (**7**) is formed by the interaction between **1** and **2**. The complex **7** has the CH···O hydrogen bond, with a distance of 1.64 Å (see Figure 4) and is essentially equienergetic to **3**. Complex **7** changes into a tetrahedral intermediate (**9**) through transition state **8**. The **G**$^-$**G**$^-$ transition state **8** is 1.6 kcal/mol above the **AG**$^-$ transition state **4**. The angle of attack ($O_1C_3O_3$) is 99°. The **G**$^-$**G**$^-$ intermediate **9** is 2.9 kcal/mol above the **AG**$^-$ **5**. The $O_1C_3O_3$ angle shifts to 110° in **9**, and the dihedral angle $O_3C_3O_2C_2$ changes to 39°. The second transition state (**10**) is also **G**$^-$**G**$^-$ but is 1.3 kcal/mol above **8**. The difference between **8** and **10** implies that the attack of methoxide on an (*Z*)-ester is preferred over methoxide attack on an unfavorable (*E*)-ester.[8a]

In the aqueous and nonpolar environments, the $\Delta G^{\ddagger}$ values for **8** become 11.0 and 6.9 kcal/mol, respectively. The solvation effects make **8** more stable than **4**; however, the activation barrier for **10** is still higher than that for **4**. Solvation stabilizes

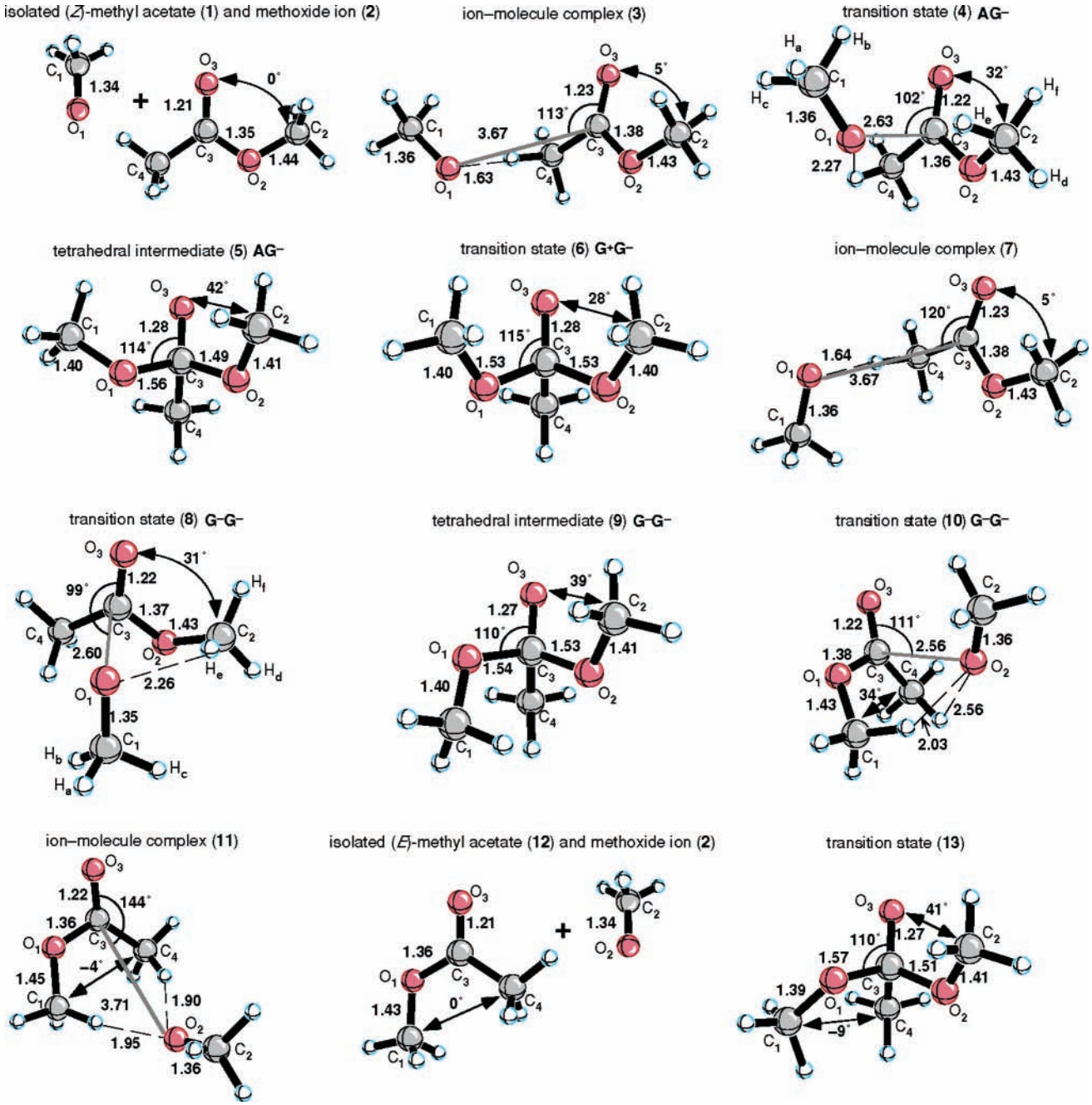

Figure 4. B3LYP/6-31+G(d) geometries of reactants, ion−molecule complexes, transition states, intermediates, and products in the transacylation of methyl acetate by methoxide. Distances are given in angstroms.

intermediate **9**, relative to the transition state, and the difference between **8** and **10** is enhanced.

Combination of the reaction pathways involving $\mathbf{AG}^-$ and $\mathbf{G}^-\mathbf{G}^-$ intermediates (Figure 3A and B) provides the third possible pathway, as shown in Figure 3C. This pathway is the lowest in energy in water and nonpolar solvents. The $\mathbf{G}^-\mathbf{G}^-$ intermediate **9** can form the $\mathbf{AG}^-$ one (**5**) by rotation of the $\mathbf{G}^-$-methoxy group (O_1Me) through the transition state **13**. The rotational barrier (4.5 kcal/mol in water) for the conversion of **9** to **5** is much smaller than the cleavage barrier (9.9 kcal/mol in water) of **9** to **11**. The intermediate **5** can be converted to **5′** via the TS2 (**6**), the anti-methoxy group (O_2Me) of **5′** can rotate to the $\mathbf{G}^+\mathbf{G}^+$ intermediate **9′** (a mirror image of **9**), and the methoxy group can dissociate to give **1** and **2**.

The transacylation pathway via the $\mathbf{AG}^-$ tetrahedral intermediate (Figure 3A) is favorable in the gas phase, whereas the pathway via both the $\mathbf{G}^-\mathbf{G}^-$ and $\mathbf{AG}^-$ tetrahedral intermediates (Figure 3C) is favored in the aqueous and nonpolar solvents.

The Origin of the Conformational Preferences of Transition States and Intermediates. We have analyzed the conformational preferences in the transition state and intermediates of the transacylation. The symmetrical intermediate, 1,1-dimethoxyethoxide, has six distinct conformers, three of which are chiral. We attempted full optimizations of all six initial structures, but after optimization, only the $\mathbf{AG}^-$ and $\mathbf{G}^-\mathbf{G}^-$ conformers are observed to be energy minima (Figure 5). The $\mathbf{AG}^-$ conformer is inherently more stable; however, the energy preference reverses in water. The $\mathbf{G}^+\mathbf{G}^-$ conformation is a transition state for interconversion of two enantiomeric $\mathbf{AG}^-$ and $\mathbf{G}^+\mathbf{A}$ minima and is only 1.1 kcal/mol higher in energy. This is quite different from the conformational preference of 1,1-dimethoxyethane, which favors a $\mathbf{G}^-\mathbf{G}^-$ conformation.[19]

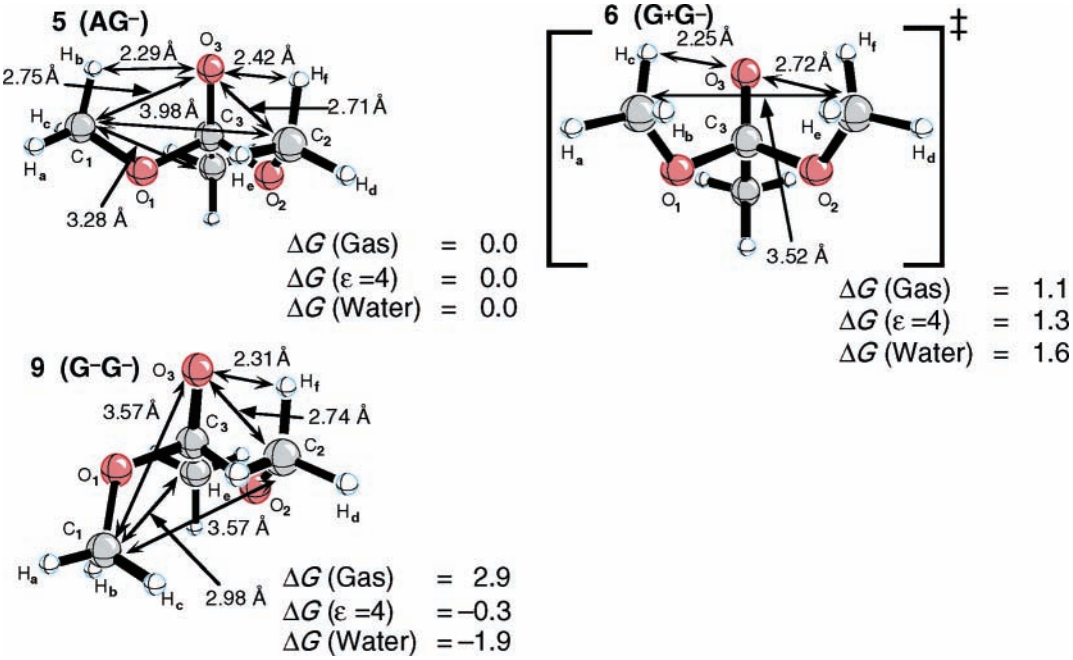

Figure 5. Optimized conformations and the relative Gibbs free energies of 1,1-dimethoxyethoxide (**5** and **9**) and $\mathbf{G}^+\mathbf{G}^-$ transition state **6**.

TABLE 2: Geometrical Parameters for the Optimized Conformers of 1,1-Dimethoxyethoxide and Dimethyl Methylphosphonate (X = C or P)[a]

	1,1-Dimethoxy-ethoxide			Dimethyl Methylphosphonate			
	AG⁻	**G⁻G⁻**	**G⁺G⁻**[b]	**AG⁻**	**G⁺G⁻**	**G⁻G⁻**	**G⁻G⁺**
			Bond Lengths (Å)				
O_1X_3	1.56	1.54	1.53	1.63	1.63	1.63	1.63
O_2X_3	1.49	1.53	1.53	1.62	1.63	1.63	1.63
O_3X_3	1.28	1.27	1.28	1.49	1.49	1.49	1.48
			Dihedral Bond Angles (deg)				
$O_3X_3O_1C_1$	30	−174	−28	25	−29	−174	175
$O_3X_3O_2C_2$	42	39	28	48	29	35	−175
			Bond Angles (deg)				
$O_1X_3O_2$	100	104	103	102	106	105	108
$O_1X_3O_3$	114	110	115	114	114	111	111
$O_2X_3O_3$	116	115	115	117	114	116	111
$C_1O_1X_3$	114	118	115	121	121	124	128
$C_2O_2X_3$	113	113	115	120	121	119	128

[a] The geometries were optimized with the B3LYP/6-31+G(d). The site numbers are shown in Figure 2. [b] Transition state for the interconversion between **5** and **5′**.

Optimized geometrical parameters of the $\mathbf{AG}^-$, $\mathbf{G}^-\mathbf{G}^-$, and $\mathbf{G}^+\mathbf{G}^-$ conformers are collected in Table 2. In the $\mathbf{AG}^-$ conformer, the O_2C_3 bond is shorter than the O_1C_3 bond, which is the result of a strong anomeric effect.[19] The bond length O_2C_3 is similar to that of O_1C_3 in the $\mathbf{G}^-\mathbf{G}^-$ conformer. However, these C−O bonds interact differently with the C−O^- bond and the O^- lone pairs. The $O_1C_3O_2$ bond angle is 4° smaller in the $\mathbf{AG}^-$ conformer than in the $\mathbf{G}^-\mathbf{G}^-$ conformer, whereas the $O_1C_3O_3$ bond angles are 4° larger, indicating that the lone pairs of the **A**-methoxy and $\mathbf{G}^-$-methoxy groups (O_1Me) interact with C−O^- and C−OMe pairs, respectively. The $\mathbf{G}^+\mathbf{G}^-$ conformer has a symmetrical structure; the O_2C_3 bond is the same length as the O_1C_3, and the $O_1C_3O_3$ angle is equal to the $O_2C_3O_3$. The $O_1C_3O_2$ bond angle is 3° larger in the $\mathbf{G}^+\mathbf{G}^-$ conformer than in the $\mathbf{AG}^-$, and the $O_1C_3O_3$ bond angles are 5° larger than those in the $\mathbf{G}^-\mathbf{G}^-$ conformer, showing that the lone pairs of the $\mathbf{G}^+$-methoxy group (O_1Me) interact with both C−O^- and C−OMe pairs.

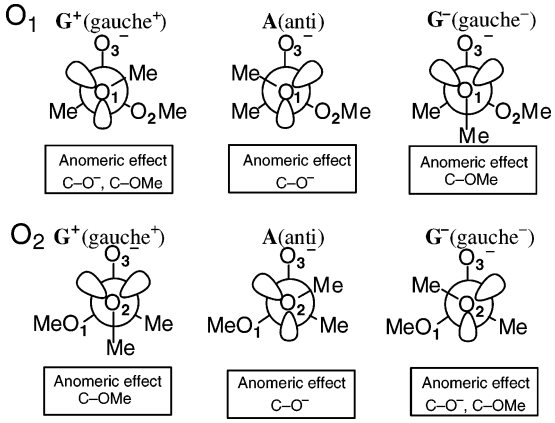

Figure 6. Orbital interactions between lp(O) oxygen lone pairs with σ^*(C−O^-), σ^*(C−OMe) of $\mathbf{G}^+$, **A**, and $\mathbf{G}^-$ conformations of 1,1-dimethoxyethoxide.

To understand the origin of the stability of these conformations and their difference in energy, the lp(O)−σ^* hyperconjugation effects were investigated qualitatively. Figure 6 shows Newman projections along the two methoxy bonds looking from oxygen toward the central carbon of the intermediate. These diagrams also show the relationships of the methyl groups and the alkoxy oxygen. The lone pairs on the front oxygen are shown as equivalent hybrid orbitals. In addition to the OMe···OMe interactions that are also present in 1,1-dimethoxyethane, the tetrahedral intermediate also has OMe···O^- interactions, as shown in Figure 6. The $\mathbf{G}^+$ conformation of O_1C_1 and the $\mathbf{G}^-$ conformation of O_2C_2 involve antiperiplanar orbital interactions between a methoxy lp(O) and both σ^*(C−O^-) and σ^*(C−OMe) orbitals. The $\mathbf{G}^-$ conformation of O_1C_1 and the $\mathbf{G}^+$ conformation of O_2C_2 afford antiperiplanar orbital interactions between the lp(O) and the σ^*(C−OMe), but not the σ^*(C−O^-). The **A** conformation gives the antiperiplanar orbital interactions between the lone pair and the σ^*(C−O^-), but not the σ^*(C−OMe).

Table 3 shows the number of the orbital interactions of lp(O) oxygen lone pairs with σ^*(C−O^-) and σ^*(C−OMe) in each conformation.[21] The $\mathbf{G}^+\mathbf{G}^-$ conformation provides the largest stabilization energy, resulting from four lp(O)−σ^* interactions,

TABLE 3: Number of Orbital Interactions between lp(O) Oxygen Lone Pairs with σ^*(X−O) and σ^*(X−OMe) (X = C or P)

	lp(O) → σ^*(X−O)	lp(O) → σ^*(X−OMe)	total
G$^+$G$^-$	2	2	4
AG$^-$	2	1	3
G$^-$G$^-$	1	2	3
AA	2	0	2
G$^-$A	1	1	2
G$^-$G$^+$	0	2	2

TABLE 4: NPA Charge Densities for the Conformers of 1,1-Dimethoxyethoxide and Dimethyl Methylphosphonate in the Gas Phase (X = C or P)[a]

		O_1	O_2	O_3	H_a	H_b	H_c	H_d	H_e	H_f
Rate-Determining Transition State										
AG$^-$	**4**	−0.96	−0.59	−0.66	0.11	0.12	0.11	0.19	0.26	0.20
G$^-$G$^-$	**8**	−0.94	−0.59	−0.65	0.12	0.09	0.10	0.20	0.27	0.20
1,1-Dimethoxyethoxide (Tetrahedral Intermediate and Transition State)										
AG$^-$	**5**	−0.69	−0.66	−0.87	0.16	0.21	0.18	0.18	0.19	0.21
G$^-$G$^-$	**9**	−0.67	−0.69	−0.85	0.19	0.16	0.20	0.18	0.17	0.22
G$^+$G$^-$[b]	**6**	−0.68	−0.68	−0.87	0.18	0.16	0.22	0.18	0.16	0.22
Dimethyl Methylphosphonate										
AG$^-$		−0.87	−0.86	−1.10	0.23	0.23	0.21	0.23	0.22	0.23
G$^+$G$^-$		−0.87	−0.87	−1.10	0.23	0.21	0.23	0.23	0.21	0.23
G$^-$G$^-$		−0.86	−0.87	−1.08	0.24	0.21	0.22	0.23	0.21	0.24
G$^-$G$^+$		−0.86	−0.86	−1.07	0.24	0.20	0.21	0.24	0.20	0.21

[a] The site numbers are shown in Figures 2, 4, 5, and 8. [b] Transition state for the interconversion.

whereas both **AG$^-$** and **G$^-$G$^-$** have three interactions and the second largest stabilization energies. Conformational preference of the **AG$^-$** conformer to the **G$^-$G$^-$** conformer shows that the orbital interactions of the lp(O) oxygen lone pair with σ^*(C−O$^-$) is larger than that of the lp(O) oxygen lone pair with σ^*(C−OMe),[19] because the C−O$^-$ component has stronger anionic character than the C−OMe component.

In addition to the hyperconjugation, electrostatic effects influence the energies of different conformers of 1,1-dimethoxyethoxide. These can be further classified as dipole−dipole interactions and CH···O hydrogen-bond effects.[18] The dipole moment of the **G$^-$G$^-$** (4.1 D) is twice more than that of the **AG$^-$** (1.6 D) and **G$^+$G$^-$** (1.8 D). The dipole−dipole interaction energies contribute to the relative stability of the **AG$^-$** and **G$^+$G$^-$** conformers in the gas phase. The difference in dipole moments is clearly a result of the lone-pair density of the two methoxy groups of the **AG$^-$** and **G$^+$G$^-$** pointing away from the highest electron density on the alkoxide oxygen. In the **G$^-$G$^-$** conformer, one of the methoxy oxygen lone pairs is pointed toward the alkoxy oxygen, increasing the dipole moment.

To evaluate possible CH···O hydrogen-bonding effects, the charge densities on the O_3 anion and H atoms in the methoxy group were calculated by natural population analysis (NPA).[21] The NPA charge densities are collected in Table 4, and the distances between relevant atoms are displayed in Figure 5. The **AG$^-$** and **G$^+$G$^-$** conformers have two short distances between the carbonyl O_3 and the H atoms ($C_1H_b\cdots O_3$ and $C_2H_f\cdots O_3$ for **AG$^-$** and $C_1H_c\cdots O_3$ and $C_2H_f\cdots O_3$ for **G$^+$G$^-$**). The O_3C_1 and O_3C_2 lengths are shorter than the general distance (C···O, 3.0−4.0 Å) of the CH···O contacts estimated by Taylor and Kennard.[18c] Because they investigated the CH···O bonds in crystals—that is, intermolecular CH···O bonds—it is not surprising that the C···O distances are shorter in the intramolecular CH···O bonds. The charge densities on the nearest H atoms to the O_3 anion are more positive than those on other H atoms, indicating that the **AG$^-$** and **G$^+$G$^-$** conformers have two intra CH···O bonds, contributing to the conformational stability. The **G$^-$G$^-$** conformer shows only one intra CH···O bond ($C_2H_f\cdots O_3$). The CH···O bond contributes to the conformational preference of the **AG$^-$** and **G$^+$G$^-$** conformers to the **G$^-$G$^-$** conformer. In contrast to 1,1-dimethoxyethane,[19b−d] 1,1-dimethoxyethoxide prefers the **AG$^-$** and **G$^+$G$^-$** conformations to the **G$^-$G$^-$** conformation in energy, because of the hyperconjugation effect between the methoxy groups and the O_3 anion and the electrostatic effects.

Steric effects were assessed from the distances between methoxy, methyl, and O$^-$ groups. As shown in Figure 5, the O_3C_1 and O_3C_2 distances are 2.75 and 2.71 Å for the **AG$^-$** conformer, 3.57 and 2.74 Å for the **G$^-$G$^-$** conformer, 2.72 and 2.72 Å for the **G$^+$G$^-$** conformer, respectively. The steric effects between a methoxy group and an O anion ($O_3\cdots C_2$) for the **AG$^-$** and **G$^+$G$^-$** conformers are similar to that for the **G$^-$G$^-$** conformer, whereas the other methoxy group and O anion ($O_3\cdots C_1$) for the **AG$^-$** and **G$^+$G$^-$** provide larger steric effects than for the **G$^-$G$^-$** conformer. However, earlier work by Venkatesan et al.[19b−d] implied that the substitution of methyl group for the hydrogen on the central C atom of 1,1-dimethoxymethane had no effect on the relative energies of the conformers. The van der Waals radius of oxygen (1.52 Å)[22] is smaller than that of methyl group (2.0 Å);[22] therefore, the steric effect contributes to the conformational preference of 1,1-dimethoxyethoxide less than hyperconjugation and electrostatic effects. Because of the van der Waals radius of a methyl group (2.0 Å),[22] the **G$^+$G$^-$** conformer provides steric repulsion between methoxy groups ($C_1\cdots C_2 = 3.52$ Å); however, the **AG$^-$** conformer sets the distance of the methoxy groups at the sum of the van der Waals radii ($C_1\cdots C_2 = 3.99$ Å) and gains stability by the van der Waals interaction. Moreover, the **G$^+$G$^-$** conformer has a smaller entropy (see Table 1) and its entropy is probably easy to change, relative to that of the more stable **AG$^-$** or **G$^+$A** (mirror image of the **AG$^-$**), because of the similarity of the structures. That is why the **G$^+$G$^-$** conformer is the transition state **6** of the interconversion between intermediates **5** (**AG$^-$**) and **5′** (**G$^+$A**).

Several studies on the influence of the solvent on the anomeric effect have been reported.[23,24] The presence of a polar solvent did not significantly reduce the preference for the conformers stabilized by an anomeric effect. Whereas the **AG$^-$** conformer is more stable in the gas phase, the **G$^-$G$^-$** conformer becomes ∼2 kcal/mol more stable than the **AG$^-$** conformer in water. The **G$^-$G$^-$** conformer (6.0 D) has ∼3 times larger dipole moment of **AG$^-$** (2.4D) and gains more electrostatic stabilization in the aqueous environment. In a protein environment, the two conformers have the same energy. A polar solvent exerts a small effect on the conformational preference of the neutral species[23,24] but has a large effect on the anionic species, because of the strong electrostatic solute−solvent interactions.

Conformations of Phosphonates and Enzyme-Bound Phosphonate Inhibitors

Phosphonate Inhibitors of Lipases and Esterases. The crystallographic structures of lipases and esterases include covalently bound inhibitors. These inhibitors are normally phosphonates and their esters.[4] Figure 1 shows different phosphonate inhibitors that are bound to lipases and esterases. The conformations of the bound inhibitors are quite similar. Figure 7 summarizes all this information to show the similarities between binding sites.[5b] A covalent bond is formed between the nucleophilic O_γ of the Ser residue and the P atom of the

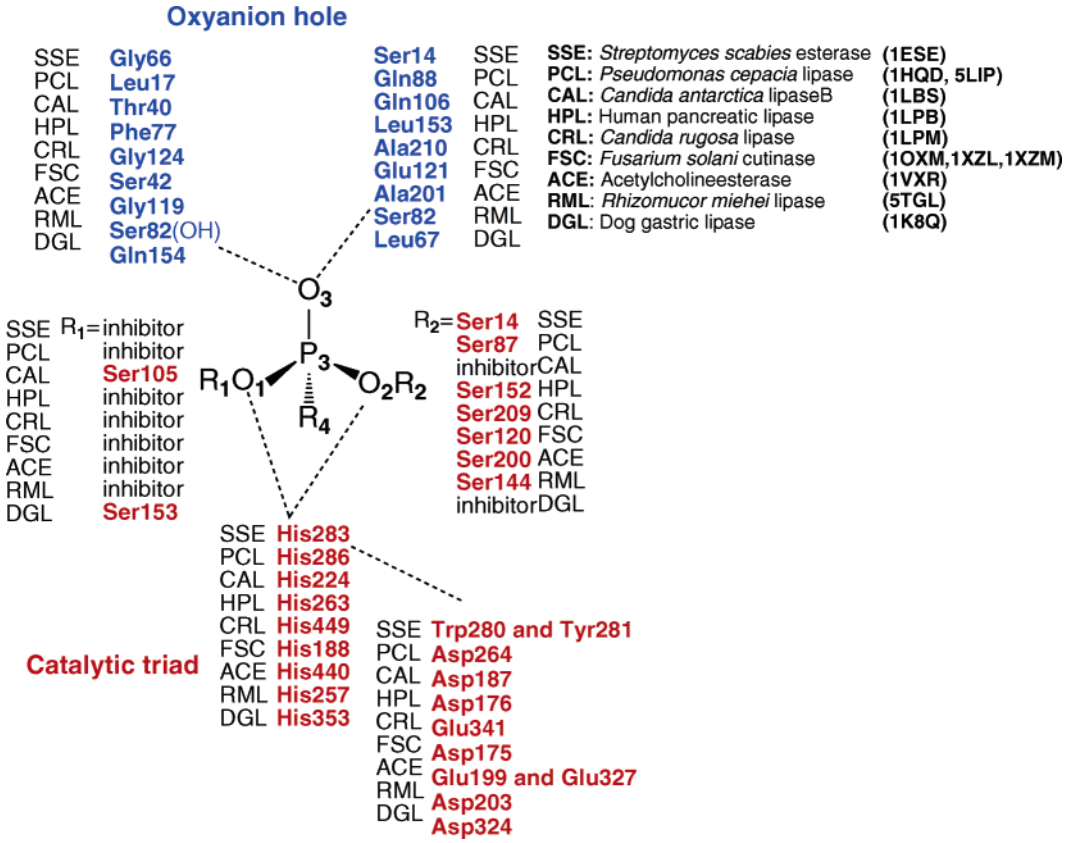

Figure 7. Residues that constitute an oxyanion hole (blue) and a catalytic triad (red) in the trans-acylation of lipases and esterases for which crystal structures are available.

TABLE 5: Geometrical Parameters for the Phosphonate-Inhibited Lipases[a,b]

		Bond Length (Å)				Bond Angle (deg)			Dihedral Bond Angle (deg)	
		P_3O_1	P_3O_2	P_3O_3	C_1C_2	$O_1P_3O_2$	$C_1O_1P_3$	$C_2O_2P_3$	$O_3P_3O_1C_1$	$O_3P_3O_2C_2$
1ESE	$\mathbf{G^+G^-}$	1.67	1.68	1.31	3.20	75	150	123	−39	+15
1HDQ	$\mathbf{AG^-}$	1.61	1.55	1.56	4.61	108	128	130	+11	+9
1K8Q	**AA**	1.58	1.63	1.60	4.87	107	120	122	+2	−45
1LBS	$\mathbf{AG^-}$	1.56	1.53	1.52	4.48	109	120	132	+55	+81
1LPB	$\mathbf{G^+G^-}$	1.67	1.60	1.59	3.62	119	125	107	−49	+40
1LPM	$\mathbf{AG^-}$	1.62	1.55	1.43	4.14	106	124	122	+4	+54
1OXM	$\mathbf{G^+G^-}$	1.59	1.60	1.57	3.74	106	127	108	−66	+31
1VXR	$\mathbf{AG^-}$	1.43	1.57	1.47	4.78	116	126	126	+41	+38
1XZL	$\mathbf{G^-G^-}$	1.62	1.62	1.60	3.89	113	123	117	+151	+48
1XZM	$\mathbf{G^-G^-}$	1.62	1.62	1.59	3.49	112	123	117	−174	+76
5LIP	$\mathbf{AG^-}$	1.57	1.57	1.47	3.88	98	123	109	+23	+34
inhibitor **1**[b]	$\mathbf{G^+G^-}$	1.59	1.59	1.51	3.55	113	112	121	−45	+43
inhibitor **2**[b]	$\mathbf{G^+G^-}$	1.60	1.61	1.50	3.43	107	112	118	−54	+43
inhibitor **3**[b]	$\mathbf{G^+G^-}$	1.57	1.60	1.49	3.75	110	112	123	−40	+37

[a] The geometries were obtained the X-ray crystallographic structure of the lipase-inhibitor complexes. The site numbers are shown in Figure 4. [b] Data taken from ref 4n.

inhibitor. In most of lipases and esterases, the Ser residue attacks the inhibitors from the *re* face, as shown in Figure 1. The alkyl chain of these inhibitors (R_4) lies in the hydrophobic groove, opposite His of the catalytic triad. Phosphonate inhibitors could adopt nine different conformers in an unsymmetrical case; however, the known bound phosphonate inhibitors are mainly in the $\mathbf{G^+G^-}$ and $\mathbf{AG^-}$ conformations, whereas the $\mathbf{G^-G^-}$ and **AA** conformations are rare. Moreover, the geometry of the **AA** is close to $\mathbf{G^+A}$, because the dihedral angle ($O_3P_3O_1C_1$) is ∼2°. Other possible conformations have not been observed in crystal structures.

The geometrical parameters of the inhibitors are summarized in Table 5. Although the parameters are distributed over a wide range, the inhibitors generally have larger bond lengths (P−O) and bond angles (OPO and POC) than the C−O lengths and the OCO or COC angles in 1,1-dimethoxyethoxide, implying the longer distance between the methyl groups ($C_1\cdots C_2$). This expansion of the distance between the O atoms reduces steric hindrance, leading to the stabilization of the $\mathbf{G^+G^-}$ conformation. The $\mathbf{G^+G^-}$ conformation in the inhibitors becomes stable, to maximize the anomeric effects around both P−O bonds.

Unbound Phosphonate Inhibitors. To compare the conformational relationship between the unbound phosphonate and the phosphonate inhibitors, the conformational preference of dimethyl methylphosphonate has also been explored. All possible conformers were fully optimized. Four minima were observed, corresponding to $\mathbf{G^+G^-}$, $\mathbf{AG^-}$ (equivalent to $\mathbf{G^+A}$), $\mathbf{G^-G^-}$ ($\mathbf{G^+G^+}$), and $\mathbf{G^-G^+}$ conformers as shown in Figure 8.[25]

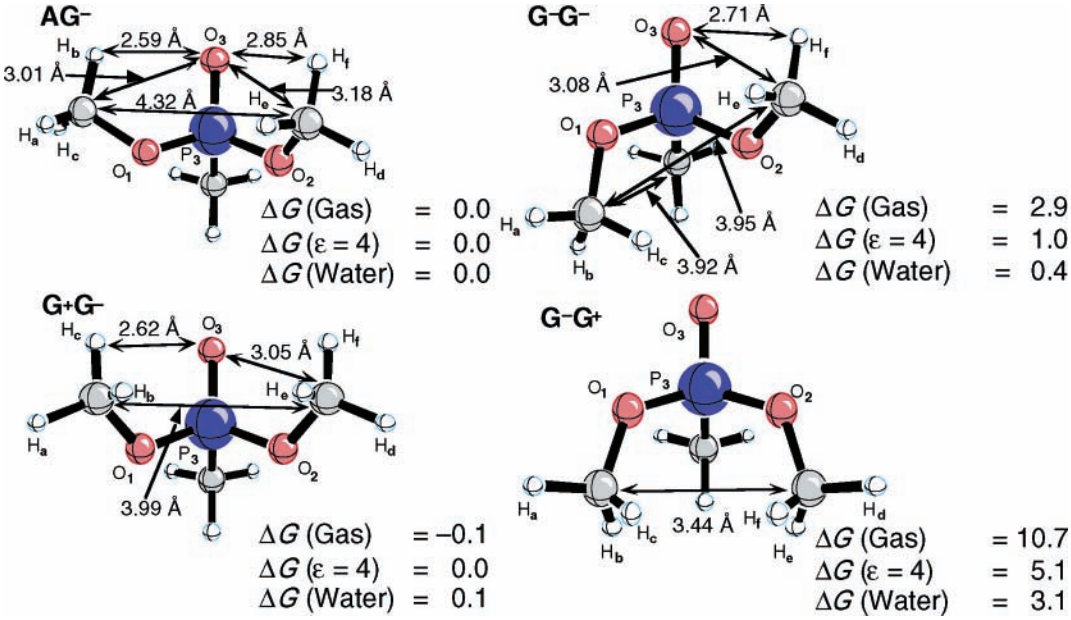

Figure 8. Optimized conformations and relative Gibbs free energies of dimethyl methylphosphonate with the relative energies of conformers.

The $\mathbf{G}^+\mathbf{G}^-$ and $\mathbf{AG}^-$ conformations have almost identical energies, indicating that the interconversion between the $\mathbf{G}^+\mathbf{G}^-$ and $\mathbf{AG}^-$ conformations probably occurs very easily. The $\mathbf{G}^-\mathbf{G}^-$ and $\mathbf{G}^-\mathbf{G}^+$ conformers are 2.9 and 10.7 kcal/mol less stable. The optimized geometries are shown in Table 2. Compared to the 1,1-dimethoxyethoxide, dimethyl methylphosphonate has longer P−O bonds and larger POC angles. However, the geometrical parameters of the dimethyl methylphosphonate, especially dihedral angles, are rather different from those of the phosphonate inhibitors, because of the substituents or the shape of the cavity in the active site.

In contrast to 1,1-dimethoxyethoxide, the $\mathbf{G}^+\mathbf{G}^-$ conformer of dimethyl methylphosphonate has methyl groups separated by the sum of the van der Waals radii ($C_1\cdots C_2 = 3.99$ Å) (see Figure 7). In the nonpolar solvent, the energy differences of the $\mathbf{G}^-\mathbf{G}^-$ and $\mathbf{G}^-\mathbf{G}^+$ conformers, with respect to the $\mathbf{G}^+\mathbf{G}^-$ conformer, decrease to 1.0 and 5.1 kcal/mol, respectively, but the order of the stabilities does not change. In water, the $\mathbf{AG}^-$ and $\mathbf{G}^+\mathbf{G}^-$ conformers are the most stable. However, the energy difference between the $\mathbf{AG}^-$ and $\mathbf{G}^-\mathbf{G}^-$ conformers is very small ($\Delta G = 0.4$ kcal/mol), implying that the conformations of dimethyl phosphonate would easily change between the $\mathbf{AG}^-$, $\mathbf{G}^+\mathbf{G}^-$, and $\mathbf{G}^-\mathbf{G}^-$ conformers in water.

Florián, Strajbl, and Warshel investigated the conformations of dimethyl methylphosphonate with MP2/6-31+G(d,p)//HF/6-31G calculations.[26] The $\mathbf{G}^+\mathbf{G}^-$ conformation was determined to be the most stable, whereas the differences in free energy of the $\mathbf{AG}^-$ and $\mathbf{G}^-\mathbf{G}^-$ conformers were 0.6 and 3.1 kcal/mol higher, in good agreement with our results. They also estimated the relative solvation free energy at the MP2/6-31+G(d,p) level, using the iterative Langevin dipoles solvation model.[27] The $\mathbf{G}^-\mathbf{G}^-$ conformation represents the global minimum in aqueous solution. The differences in free energy of the $\mathbf{AG}^-$ and $\mathbf{G}^+\mathbf{G}^-$ conformers are slightly higher ($\Delta\Delta G = 0.2$ and 0.5 kcal/mol, respectively); however, the energy differences are less than the uncertainty in the Gibbs free energies that they have computed (0.7 kcal/mol). The order of the stability of the conformers in aqueous solution is similar to that in this work but are not exactly the same, because of the differences in the solvation models.

Comparisons between Free Phosphonate, Phosphonate Inhibitors, and the Transition State of the Transacylation of Methyl Acetate

Several previous computational studies have examined the structures of transition-state analogues (TSAs) and compared them with various tetrahedral intermediates and transition states.[5a−5i] Mader and Bartlett reviewed TSAs and their references to catalytic antibodies.[5a] TSAs of various proteases and catalytic antibodies were investigated by Houk and co-workers, using ab initio calculations.[5b−d] Various TSAs, which function as inhibitors of a β-lactamase, were examined by Curley and Pratt, using force field calculations.[5e] Comparisons of MP2/6-31+G(d) structures of tetrahedral intermediates and phosphonate TSAs involved in methyl acetate hydrolysis were reported by Teranishi and co-workers.[5f] Ohkubo and co-workers reported a similar study at a lower level of theory and applied TSAs to make cross-linked polymers, which catalyze the hydrolysis of esters.[5g−i]

Table 6 summarizes the relative energies of phosphonates and compares these values to those of the transition states and intermediates for the transacylation of methyl acetate in various media. The transition state for the methoxide attack, and presumably also that for base-promoted serine attack, has the $\mathbf{AG}^-$ conformation (**4**). The $\mathbf{G}^-\mathbf{G}^-$ conformer (**8**) is higher in energy. In the solvent model, the $\mathbf{G}^-\mathbf{G}^-$ conformer becomes the lowest in energy, because of the strong electrostatic interactions of anion species. Because of the role of the anomeric effect in both cases, the transition state (**6**) and intermediates (**5** and **9**) share the $\mathbf{G}^+\mathbf{G}^-$, $\mathbf{AG}^-$, and $\mathbf{G}^-\mathbf{G}^-$ conformations as the low-energy conformers.

Phosphonates have the same low-energy conformers and can readily achieve only the $\mathbf{G}^+\mathbf{G}^-$, $\mathbf{AG}^-$, and $\mathbf{G}^-\mathbf{G}^-$ conformers. It is not surprising that the conformations are present in available crystal structures. Unbound phosphonates in the gas phase exhibit the same conformational preference, $\mathbf{G}^+\mathbf{G}^-$ > $\mathbf{AG}^-$ ($\mathbf{G}^+\mathbf{A}$) > $\mathbf{G}^-\mathbf{G}^-$ ($\mathbf{G}^+\mathbf{G}^+$), as the enzyme bound phosphonates, showing that the binding pockets of lipases and esterases are probably nonpolar and large. The $\mathbf{G}^+\mathbf{G}^-$ and $\mathbf{AG}^-$ conformations are the most stable; no change of the order of conformational stability is observed, in contrast to the transacylation of methyl acetate. The P−O bond distances in the

TABLE 6: Relative Energies of the Conformers of the Transitions States and Intermediates of the Transacylation of Methyl Acetate and the Unbound and Bound Phosphonates

	$MeO^- + MeCO_2Me$						Phosphonate			
	Transition State			Intermediate			Dimethyl Methylphosphonate			
	gas	$\epsilon = 4$	water	gas	$\epsilon = 4$	water	gas	$\epsilon = 4$	water	number of bound inhibitors
$\mathbf{G^+G^-}$				1.1[a]	1.6[a]	3.5[a]	0	0	0.1	7
$\mathbf{AG^-}$	0	1.2	3.1	0	0.3	1.9	0.1	0	0	5
$\mathbf{G^-G^-}$	1.6	0	0	2.9	0	0	2.9	1.0	0.4	2
$\mathbf{G^-G^+}$							10.7	5.1	3.1	
AA										1

[a] Transition state for the interconversion between $\mathbf{AG^-}$ and $\mathbf{G^+A}$ intermediates.

phosphonates are different from the C−O bond distances in the tetrahedral intermediates and transition states (see Tables 2 and 5). NPA charges of the conformers of 1,1-dimethoxyethoxide and dimethyl methylphosphonate in the gas phase (Table 4) provide additional insights into the relationship between the phosphonate inhibitors and the tetrahedral intermediates and transition states. Examination of the partial charges reveals that dimethyl methylphosphonate does not mimic the rate-determining transition states **4** and **8**, with regard to the charge density.

Although the low-energy conformers ($\mathbf{G^+G^-}$, $\mathbf{AG^-}$, and $\mathbf{G^-G^-}$) are common to the phosphonates and to the nucleophilic addition transition states, the most common bound phosphonate conformer ($\mathbf{G^+G^-}$) is different from the lowest-energy transacylation transition state ($\mathbf{AG^-}$).

The preferred conformers of the bound inhibitors more resemble the geometries of transition states or phosphonate conformational minima than stable conformations of the tetrahedral intermediates of transacylations.

Conclusion

Conformational analyses have been performed for the transition states and the tetrahedral intermediates of the transacylation of methyl acetate and for the phosphonate models for inhibitors that are bound to lipases and esterases. The lowest-energy reaction pathway of the transacylation involves the anti gauche$^-$ ($\mathbf{AG^-}$) transition state and intermediate in the gas phase (see Figure 3A). In the conformational analysis of the intermediate of the transacylation, the $\mathbf{AG^-}$ and gauche$^-$ gauche$^-$ ($\mathbf{G^-G^-}$) conformers were only the minima found in the gas phase; however, the gauche$^+$ gauche$^-$ ($\mathbf{G^+G^-}$) transition state is only 1.1 kcal/mol above $\mathbf{AG^-}$. The preference for the $\mathbf{AG^-}$ conformer over the $\mathbf{G^-G^-}$ is different from that observed for 1,1-dimethoxyethane in the gas phase,[20] because of the hyperconjugative interaction between the lp(O) oxygen lone pairs and the σ^*(C−O$^-$) orbital. However, in the aqueous environment, the reaction pathway via both the $\mathbf{G^-G^-}$ and $\mathbf{AG^-}$ tetrahedral intermediates (see Figure 3C) is favored.

The phosphonate inhibitor structures found in lipases and esterases are seven $\mathbf{G^+G^-}$ and five $\mathbf{AG^-}$ inhibitor conformers. These closely resemble the most stable conformers of the free phosphonates in gas or solution. The $\mathbf{AG^-}$ structures also resemble the rate-determining transition state of transacylation in the gas phase. The two $\mathbf{G^-G^-}$ phosphonate inhibitors found in crystal structure correspond to the transition states calculated for transacylation in solvent. The three-dimensional shapes of the active sites of esterases and lipases accommodate inhibitors in their lowest-energy conformations rather than faithfully mimicking the rate-determining transition states of the reaction.

Acknowledgment. We are grateful to the Japan Society for the Promotion of Science for a Research Fellowship for Young Scientists Abroad to Y.T., and we are grateful to the National Institute of General Medical Sciences, National Institutes of Health, for financial support of this research. We also thank Joe Schrag and Romas J. Kazlauskas for the structures sets of several lipase-inhibitor complexes, and Professor Kazlauskas for alerting us to the interesting problem of stereoselectivity in lipase catalysis and for offering many helpful comments.

Supporting Information Available: Energies and geometries for all stationary points and NBO energies of the orbital interactions of lp(O) oxygen lone pairs with σ^*(X−O) and σ^*(X−OMe) (X = C or P) in conformations of the tetrahedral intermediate and dimethyl phosphonate (Table S1) (PDF). This material is available free of charge via the Internet at http://pubs.acs.org.

References and Notes

(1) (a) Fersht, A. *Enzyme Structure and Mechanism*, 2nd ed.; W. H. Freeman and Company: New York, 1999. (b) Sears, P.; Wong, C.-H. *Angew. Chem., Int. Ed.* **1999**, *38*, 2300−2324. (c) Gabius, H. J.; Gabius, S. *Glycosciences: Status and Perspectives*; Chapman & Hall: London, 1997. (d) Mikkelsen, L. M.; Hernáiz, M. J.; Martin-Pastor, M.; Skrydstrup, T.; Jiménez-Barbero, J. *J. Am. Chem. Soc.* **2002**, *124*, 14940−14951. (e) Almond, A.; Peterse, B. O.; Duus, J. O. *Biochemistry* **2004**, *43*, 5853−5863.

(2) (a) Hur, S.; Bruice, T. C. *Proc. Natl. Acad. Sci. U.S.A.* **2002**, *99*, 1176−1181. (b) Lightstone, F. C.; Bruice, T. C. *J. Am. Chem. Soc.* **1996**, *118*, 2595−2605. (c) Bruice, T. C.; Lightstone, F. C. *Acc. Chem. Res.* **1999**, *32*, 127−136. (d) Guimarães, C. R. W.; Repasky, M.; Chandrasekhar, J.; Tirado-Rives, J.; Jorgensen, W. L. *J. Am. Chem. Soc.* **2003**, *125*, 6892−6899. (e) Ranaghan, K. E.; Ridder, L.; Szefczyk, B.; Sokalski, W. A.; Hermann, J. C.; Mulholland, A. J. *Org. Biomol. Chem.* **2004**, *2*, 968−980.

(3) (a) Quinn, D. M.; Feaster, S. R. Esterases and Lipases. In *Comprehensive Biological Catalysis: A Mechanistic Reference*; Sinnot, M., Ed.; Academic Press: San Diego, CA, 1998; Vol. 2, Chapter 12. (b) Schmid, R. D.; Verger, R. *Angew. Chem., Int. Ed. Engl.* **1998**, *37*, 1608−1633. (c) Reetz, M. T. *Curr. Opin. Chem. Biol.* **2002**, *6*, 145−150. (d) Quinn, D.; Medhekar, R.; Baker, N. Ester Hydrolysis. In *Comprehensive Natural Products Chemistry: Enzymes, Enzyme Mechanisms, Proteins, and Aspects of NO Chemistry*; Poulter, C. D., Ed.; Elsevier Science: Oxford, U.K., 1999; pp 101−137.

(4) (a) Brzozowski, A. M.; Derewenda, U.; Derewenda, Z. S.; Dodson, G. G.; Lawson, D. M.; Turkenburg, J. P.; Bjorkling, F.; Huge-Jensen, B.; Patkar, S. A.; Thim, L. *Nature* **1991**, *351*, 491−494. (b) Cygler, M.; Grochulski, P.; Kazlauskas, R. J.; Schrag, J. D.; Bouthillier, F.; Rubin, B.; Serreqi, A. N.; Gupta, A. K. *J. Am. Chem. Soc.* **1994**, *116*, 3180−3186. (c) Wei, Y.; Schottel, J. L.; Derewenda, U.; Swenson, L.; Patkar, S.; Derewenda, Z. S. *Nature Struct. Biol.* **1995**, *2*, 218−223. (d) Egloff, M.-P.; Marguet, F.; Buono, G.; Verger, R.; Cambillau, C.; van Tilbeurgh, H. *Biochemistry* **1995**, *34*, 2751−2762. (e) Uppenberg, J.; Öhrner, N.; Norin, M.; Hult, K.; Kleywegt, G. J.; Patkar, S.; Waagen, V.; Anthonsen, T.; Jones, T. A. *Biochemistry* **1995**, *34*, 16838−16851. (f) Weissfloch, A. N. E.; Kazlauskas, R. J. *J. Org. Chem.* **1995**, *60*, 6959−6969. (g) Longhi, S.; Mannesse, M.; Verheij, H. M.; De Haas, G. H.; Egmond, M.; Knoops-Mouthuy, E.; Cambillau, C. *Protein Sci.* **1997**, *6*, 275−286. (h) Schrag, J. D.; Li, Y.; Cygler, M.; Lang, D.; Burgdorf, T.; Hecht, H.-J.; Schmid, R.; Schomburg, D.; Rydel, T. J.; Oliber, J. D.; Strickland, L. C.; Dunaway, C. M.; Larson, S. B.; Day, J.; McPherson, A. *Structure* **1997**, *5*, 187−202. (i) Lang, D.

A.; Mannesse, M. L. M.; De Haas, G. H.; Verheij, H. M.; Dijkstra, B. W. *Eur. J. Biochem.* **1998**, *254*, 333−340. (j) Millard, C. B.; Koellner, G.; Ordentlich, A.; Shafferman, A.; Silman, I.; Sussman, J. L. *J. Am. Chem. Soc.* **1999**, *121*, 9883−9884. (k) Tuomi, W. V.; Kazlauskas, R. J. *J. Org. Chem.* **1999**, *64*, 2638−2647. (l) Luic, M.; Tomic, S.; Lescic, I.; Ljubovic, E.; Sepac, D.; Sunjic, V.; Vitale, L.; Saenger, W.; Kojic-Prodic, B. *Eur. J. Biochem.* **2001**, *268*, 3964−3973. (m) Roussel, A.; Miled, N.; Berti-Dupuis, L.; Riviere, M.; Spinelli, S.; Berna, P.; Gruber, V.; Verger, R.; Cambillau, C. *J. Biol. Chem.* **2002**, *277*, 2266−2274. (n) Mezzetti, A.; Schrag, J. D.; Cheong, C. S.; Cygler, M.; Malardier-Jugroot, C.; Whitehead, M. A.; Kazlauskas, R. J. *ChemBioChem*, submitted.

(5) (a) Mader, M. M.; Bartlett, P. A. *Chem. Rev.* **1997**, *97*, 1281−1301. (b) Tantillo, D. J.; Houk, K. N. *Chem. Biol.* **2001**, *8*, 535−545. (c) Tantillo, D. J.; Houk, K. N. *J. Org. Chem.* **1999**, *64*, 3066−3076. (d) Radkiewicz, J. L.; McAllister, M. A.; Goldstein, E.; Houk, K. N. *J. Org. Chem.* **1998**, *63*, 1419−1428. (e) Curley, K.; Pratt, R. F. *J. Am. Chem. Soc.* **1997**, *119*, 1281−1301. (f) Teranishi, K.; Saito, M.; Fujii, I.; Nakamura, H. *Tetrahedron Lett.* **1992**, *33*, 7153−7156. (g) Ohkubo, K.; Urata, Y.; Seri, K.; Ishida, H.; Sagawa, T.; Nakashima, T.; Imagawa, Y. *J. Mol. Catal.* **1994**, *90*, 355−365. (h) Ohkubo, K.; Sawakuma, K.; Sagawa, T. *Polymer* **2001**, *42*, 2263−2266. (i) Ohkubo, K.; Sawakuma, K.; Sagawa, T. *J. Mol. Catal. A* **2001**, *165*, 1−7.

(6) (a) Warshel, A.; Narayszabo, G.; Sussman, F.; Hwang, J. K. *Biochemistry* **1989**, *28*, 3629−3637. (b) Fuxreiter, M.; Warshel, A. *J. Am. Chem. Soc.* **1978**, *100*, 8041−8047. (c) Blow, D. M.; Birktoft, J. J.; Hartley, B. S. *Nature* **1969**, *221*, 337−340. (d) Bachovchin, W. W.; Roberts, J. D. *J. Am. Chem. Soc.* **1996**, *118*, 2340−2346. (e) Massiah, M. A.; Viragh, C.; Reddy, P. M.; Kovach, I. M.; Johnson, J.; Rosenberry, T. L.; Mildvan, A. S. *Biochemistry* **2001**, *40*, 5682−5690. (f) Zhang, Y.; Kua, J.; McCammon, J. A. *J. Am. Chem. Soc.* **2002**, *124*, 10572−10577. (g) Ishida, T.; Kato, S. *J. Am. Chem. Soc.* **2003**, *125*, 12035−12048. (h) Ishida, T.; Kato, S. *J. Am. Chem. Soc.* **2004**, *126*, 7111−7118.

(7) (a) Jorgensen, W. L.; Blake, J. F.; Masura, J. D.; Wierschke, S. G. In *ACS Symposium Series 353*; American Chemical Society: Washington, DC,. 1987; p 200. (b) Dewar, M. J. S.; Storch, D. M. *J. Chem. Soc., Perkin Trans. 2* **1989**, 877−885. (c) Hori, K. *J. Chem. Soc., Perkin Trans. 2* **1992**, 1629−1633. (d) Pranata, J. *J. Phys. Chem.* **1994**, *98*, 1180−1184. (e) Hæffner, F.; Hu, C.-H.; Brinck, T.; Norin, T. *J. Mol. Struct. (THEOCHEM)* **1999**, *459*, 85−93. (f) Sherer, E. C.; Turner, G. M.; Shields, G. C. *Int. J. Quantum Chem. Quantum Biol. Symp.* **1995**, *22*, 83−93. (g) Turner, G. M.; Sherer, E. C.; Shields, G. C. *Int. J. Quantum Chem. Quantum Biol. Symp.* **1995**, *22*, 103−112. (h) Chong, L. T.; Bandyopadhyay, P.; Scanlan, T. S.; Kuntz, I. D.; Kollman, P. A. *J. Comput. Chem.* **2003**, *24*, 1371−1377. (i) Zhan, C.-G.; Landry, D. W.; Ornstein, R. L. *J. Am. Chem. Soc.* **2000**, *122*, 1522−1530. (j) Zhan, C.-G.; Landry, D. W.; Ornstein, R. L. *J. Phys. Chem. A* **2000**, *104*, 7672−7678. (k) Zhan, C.-G.; Landry, D. W.; Ornstein, R. L. *J. Am. Chem. Soc.* **2000**, *122*, 2621−2627. (l) Pliego, J. R., Jr.; Riveros, J. M. *Chem. Eur. J.* **2002**, *8*, 1945−1953. (m) Pliego, J. R., Jr.; Riveros, J. M. *Chem. Eur. J.* **2001**, *7*, 169−175. (n) Pliego, J. R., Jr.; Riveros, J. M. *J. Phys. Chem. A* **2004**, *108*, 2520−2526.

(8) (a) Deslongchamps, P. *Stereoelectronic Effects in Organic Chemistry*; Pergamon Press: New York, 1983. (b) Ema, T.; Kobayashi, J.; Maeno, S.; Sakai, T.; Utaka, M. *Bull. Chem. Soc. Jpn.* **1998**, *71*, 443−453. (c) Perrin, C. L. *Acc. Chem. Res.* **2002**, *35*, 28−34.

(9) (a) Becke, A. D. *Phys. Rev. A* **1988**, *38*, 3098−3100. (b) Lee, C.; Yang, W.; Parr, R. G. *Phys. Rev. B* **1988**, *37*, 785−789. (c) Becke, A. D. *J. Chem. Phys.* **1993**, *98*, 5648−5652.

(10) (a) Mclean, A. D.; Chandler, G. S. *J. Chem. Phys.* **1980**, *72*, 5639−5648. (b) Krishnan, R.; Binkley, J. S.; Seeger, R.; Pople, J. A. *J. Chem. Phys.* **1980**, *72*, 650−654.

(11) (a) Clark, T.; Chandrasekhar, J.; Spitznagel, G. W.; Schleyer, P. v. R. *J. Comput. Chem.* **1983**, *4*, 294−301. (b) Frisch, M. J.; Pople, J. A.; Binkley, J. S. *J. Chem. Phys.* **1984**, *80*, 3265−3269.

(12) (a) Frisch, M. J.; Trucks, G. W.; Schlegel, H. B.; Scuseria, G. E.; Robb, M. A.; Cheeseman, J. R.; Zakrzewski, V. G.; Montgomery, J. A., Jr.; Stratmann, R. E.; Burant, J. C.; Dapprich, S.; Millam, J. M.; Daniels, A. D.; Kudin, K. N.; Strain, M. C.; Farkas, O.; Tomasi, J.; Barone, V.; Cossi, M.; Cammi, R.; Mennucci, B.; Pomelli, C.; Adamo, C.; Clifford, S.; Ochterski, J.; Petersson, G. A.; Ayala, P. Y.; Cui, Q.; Morokuma, K.; Malick, D. K.; Rabuck, A. D.; Raghavachari, K.; Foresman, J. B.; Cioslowski, J.; Ortiz, J. V.; Baboul, A. G.; Stefanov, B. B.; Liu, G.; Liashenko, A.; Piskorz, P.; Komaromi, I.; Gomperts, R.; Martin, R. L.; Fox, D. J.; Keith, T.; Al-Laham, M. A.; Peng, C. Y.; Nanayakkara, A.; Challacombe, M.; Gill, P. M. W.; Johnson, B.; Chen, W.; Wong, M. W.; Andres, J. L.; Gonzalez, C.; Head-Gordon, M.; Replogle, E. S.; Pople, J. A. *Gaussian 98*, revision A.9; Gaussian, Inc.: Pittsburgh, PA, 1998. (b) Frisch, M. J.; Trucks, G. W.; Schlegel, H. B.; Scuseria, G. E.; Robb, M. A.; Cheeseman, J. R.; Montgomery, J. A., Jr.; Vreven, T.; Kudin, K. N.; Burant, J. C.; Millam, J. M.; Lyengar, S. S.; Tomasi, J.; Barone, V.; Mennucci, B.; Cossi, M.; Scalmani, G.; Rega, N.; Petersson, G. A.; Nakatsuji, H.; Hada, M.; Ehara, M.; Toyota, K.; Fukuda, R.; Hasegawa, J.; Ishida, M.; Nakajima, T.; Honda, Y.; Kitao, O.; Nakai, H.; Klene, M.; Li, X.; Knox, J. E.; Hratchian, H. P.; Cross, J. B.; Adamo, C.; Jaramillo, J.; Gomperts, R.; Stratmann, R. E.; Yazyev, O.; Austin, A. J.; Camml, R.; Pomelli, C.; Ochterski, J. W.; Ayala, P. Y.; Morokuma, K.; Voth, G. A.; Salvador, P.; Dannenberg, J. J.; Zakrzewski, V. G.; Dapprich, S.; Daniels, A. D.; Strain, M. C.; Farkas, O.; Malick, D. K.: Rabuck, A. D.; Raghavachari, K.; Foresman, J. B.; Ortiz, J. V.; Cui, Q.; Baboul, A. G.; Clifford, S.; Cioslowski, J.; Stefanov, B. B.; Liu, G.; Liashenko, A.; Piskorz, P.; Komaromi, I.; Martin, R. L.; Fox, D. J.; Keith, T.; Al-Laham, M. A.; Peng, C. Y.; Nanayakkara, A.; Challacombe, M.; Gill, P. M. W.; Johnson, B.; Chen, W.; Wong, M. W.; Gonzalez, C.; Pople, J. A. *Gaussian 03*, revision B.04; Gaussian, Inc.: Pittsburgh, PA, 2003.

(13) In the transacylation in lipases and esterases, it would be more likely that the proton of serine is pulled out as its oxygen starts to attack the ester carbonyl, because the pK_a of serine is ∼16. However, our purpose is to explore the relationship on the conformational preferences of the transition states and intermediates in transacylation to the phosphonate inhibitors. The proton transfer, itself, would not affect the conformational preference of the transacylation, because, in the transition state, the proton becomes attached to histidine.

(14) (a) Bauschlicher, C. W.; Partridge, H. *J. Chem. Phys.* **1995**, *103*, 1788−1791. (b) Wong, M. W. *Chem. Phys. Lett* **1996**, *256*, 391−399. (c) Scott, A. P.; Radom, L. *J. Phys. Chem.* **1996**, *100*, 16502−16513.

(15) (a) Miertus, S.; Scrocco, E.; Tomasi, J. *Chem. Phys.* **1981**, *55*, 117−129. (b) Barone, V.; Cammi, R.; Tomasi, J. *Chem. Phys. Lett.* **1996**, *255*, 327−335. (c) Cossi, M.; Scalmani, G.; Rega, N.; Barone, V. *J. Chem. Phys.* **2002**, *117*, 43−54. (d) Barone, V.; Improta, R.; Rega, N. *Theor. Chem. Acc.* **2004**, *111*, 237−245. (e) Takano, Y.; Houk, K. N. *J. Chem. Theory Comput.*, in press. (f) Foresman, J. B.; Keith, T. A.; Wiberg, K. B.; Snoonian, J.; Frisch, M. J. *J. Phys. Chem.* **1996**, *100*, 16098−16104.

(16) Gilson, M. K.; Honig, B. H. *Biopolymers* **1986**, *25*, 2097−2119.

(17) We also explored the concerted (S_N2) reaction path for the transacylation of methyl acetate. The activation free energies for the concerted pathway are 3.9, 10.7, and 17.1 kcal/mol in the gas phase, protein, and water; therefore, the stepwise mechanism via tetrahedral intermediate was favored to the concerted one.

(18) (a) Sutor, D. J. *Nature* **1962**, *195*, 68−69. (b) Desiraju, G. R. *Acc. Chem. Res.* **1991**, *24*, 290−296. (c) Desiraju, G. R. *Acc. Chem. Res.* **1996**, *29*, 441−449. (d) Taylor, R.; Kennard, O. *J. Am. Chem. Soc.* **1982**, *104*, 5063−5070. (e) Houk, K. N.; Menzer, S.; Newton, S. P.; Raymo, F. M.; Stoddart, J. F.; Williams, D. J. *J. Am. Chem. Soc.* **1999**, *121*, 1479−1487. (f) Takahashi, O.; Yasunaga, K.; Gondoh, Y.; Kohno, Y.; Saito, K.; Nishio, M. *Bull. Chem. Soc. Jpn.* **2002**, *75*, 1777−1783. (g) Cannizzaro, C. E.; Houk, K. N. *J. Am. Chem. Soc.* **2002**, *124*, 7163−7169.

(19) (a) *The Anomeric Effect and Associated Stereoelectronic Effects*; Thatcher, G. R. J., Ed.; ACS Symposium Series 539; American Chemical Society: Washington, DC, 1993. (b) Venkatesan, V.; Sundararajan, K.; Sankaran, K.; Viswanathan, K. S. *Spectrochim. Acta A* **2002**, *58*, 467−478. (c) Venkatesan, V.; Sundararajan, K.; Viswanathan, K. S. *J. Phys. Chem. A* **2002**, *106*, 7707−7713. (d) Venkatesan, V.; Sundararajan, K.; Viswanathan, K. S. *Spectrochim. Acta A* **2003**, *59*, 1497−1507. The definitions of the conformations of these papers are different from ours.

(20) Pliego, J. R., Jr.; Riveros, J. M. *Phys. Chem. Chem. Phys.* **2002**, *4*, 1622−1627.

(21) NBO analyses were also performed for the **AG**$^-$ and **G**$^-$**G**$^-$ conformers of 1,1-dimethoxyethoxide and dimethyl phosphonate. NBO energies of the orbital interactions of lp(O) oxygen lone pairs with σ^*(X−O) and σ^*(X−OMe) (X = C or P) are summarized in Table S1 in Supporting Information. The total NBO energy of the **AG**$^-$ conformer is larger than that of the **G**$^-$**G**$^-$ conformer. The stabilization energies for the orbital interactions of a methoxy oxygen lone pair with σ^*(C−O$^-$) and σ^*(C−OMe) are 5−6 and 4−5 kcal/mol, respectively (see Table S1). (a) Reed, A. E.; Curtiss, L. A.; Weinhold, F. *Chem. Rev.* **1988**, *88*, 899−926. (b) Glendening, E. D.; Badenhoop, J. K.; Reed, A. E.; Carpenter, J. E.; Weinhold, F. *NBO 4.M.*; Theoretical Chemistry Institute, University of Wisconsin: Madison, WI.

(22) Bondi, A. *J. Chem. Phys.* **1964**, *68*, 441−451.

(23) (a) Cramer, C. J. *J. Org. Chem.* **1992**, *57*, 7034−7043. (b) Montagnani, R.; Tomasi, J. *Int. J. Quantum Chem.* **1991**, *39*, 851−870. (c) Juaristi, E.; Cuevas, G. *Tetrahedron* **1992**, *48*, 5019−5087. (d) Alagona, G.; Bonaccorsi, R.; Tomasi, J. *J. Mol. Struct. (THEOCHEM)* **1986**, *30*, 263−277.

(24) (a) Carballeira, L.; Pérez-Juste, I. *J. Phys. Chem. A* **2000**, *104*, 9362−9369. (b) Carballeira, L.; Pérez-Juste, I. *J. Comput. Chem.* **2001**, *22*, 135−150. (c) Carballeira, L.; Pérez-Juste, I. *J. Comput. Chem.* **2000**, *21*, 462−477.

(25) Hyperconjugative effects on the conformations of dimethyl methylphosphonate were also investigated. The order of the lp(O)−σ^* stabilization energies is expected to be **G**$^+$**G**$^-$ > **AG**$^-$ > **G**$^-$**G**$^-$ > **G**$^-$**G**$^+$, as shown in Table S1 in Supporting Information. The dipole moment of the **G**$^+$**G**$^-$ conformers (2.1 D) is the same as that of **AG**$^-$ (2.2 D), half as large as that of the **G**$^-$**G**$^-$ (4.4 D), and much smaller than that of the **G**$^-$**G**$^+$ conformer (7.0 D). The dipole−dipole interactions contribute to the stabilization of the **G**$^+$**G**$^-$ and **AG**$^-$ more than the **G**$^-$**G**$^-$ and **G**$^-$**G**$^+$ in the gas phase. The charge densities of the nearest methoxy hydrogens to phosphonyl oxygen

(O_3) are similar to those of others, because of the large CH···O distances (2.6−2.8 Å); consequently, the CH···O hydrogen bonds are negligible.

(26) Florián, J.; Strajbl, M.; Warshel, A. *J. Am. Chem. Soc.* **1998**, *120*, 7959−7966.

(27) (a) Warshel, A.; Russell, S. T. *Q. Rev. Biol.* **1984**, *17*, 283−422. (b) Lee, F. S.; Chu, Z. T.; Warshel, A. *J. Comput. Chem.* **1993**, *14*, 161−185. (c) Florián, J.; Warshel, A. *J. Phys. Chem. B* **1997**, *101*, 5585−5595.